Raman, Surface Enhanced Raman Spectroscopy, and DFT Calculations: A Powerful Approach for the Identification and Characterization of 5-Fluorouracil Anticarcinogenic Drug Species

Ioana Pavel,*,†,‡ Smaranda Cota,† Simona Cîntă-Pînzaru,§ and Wolfgang Kiefer†

Institut für Physikalische Chemie, Universität Würzburg, Am Hubland, D-97074 Würzburg, Germany, Department of Chemistry and Biochemistry, University of California at Santa Barbara, Santa Barbara, California 93106-9510, and Molecular Spectroscopy Department, Babeş-Bolyai University, Kogălniceanu 1, RO-400084 Cluj-Napoca, Romania

Received: July 2, 2005; In Final Form: August 30, 2005

The normal Raman and SERS spectra of 5-fluorouracil (5-FU) in water solution and attached to a biological artificial model (a silver colloid) at different pH values were recorded and discussed. The DFT calculation results helped us to establish for the first time the most stable resonance structure for each of the tautomeric forms (i.e., two enol and two enolate forms) and to interpret the Raman and SERS spectra. At alkaline pH, both deprotonated forms of 5-FU were found to be present in solution and to adsorb on the Ag surface in a perpendicular orientation or an orientation not significantly tilted from the surface normal. The N3-deprotonated form seems to be the dominant tautomer in the adsorbed state, more probably attached through the O7 atom. At acid pH values, the N3-deprotonated form was again found to be the mainly chemisorbed species adopting a similar orientation. The combination of these two approaches (i.e., the theoretical and experimental one) proved to be a viable candidate for inclusion in a rapid, sensitive biological method of detecting and studying such essential anticarcinogenic species or biological threats in different conditions.

1. Introduction

5-Fluorouracil (5-FU) is a fluorinated pyrimidine antimetabolite (Scheme 1, R = F) that is structurally similar to uracil (Scheme 1, R = H), one of the necessary buildings block in cellular division and growth.[1−4] The well-known anticarcinogenic drug 5-FU is mostly employed in palliation of inoperable malignant neoplasms, especially those of the gastrointestinal tract, breast, liver, and pancreas.[1,5,6] 5-FU drug solutions and creams are also used to treat human skin cancer.[7,8] Moreover, all uracil compounds, in which the hydrogen bounded at the C5 atom is substituted by halogen atoms (Scheme 1, R = F, Cl, Br, I), are presently tested against HIV[1,9,10] and used as antitumor[7,8] and antiviral[10,11] drugs.

It is well-known that the pK_a value of free 5-FU is about 7.8. This was proved by titration experiments monitored by the NMR resonance of the N3 imin proton of 5-FU.[12] But we cannot rule out the possibility that the pK_a value of 5-FU may change with the environment. Conformational dependences of the pK_a value of a base are not uncommon. For example, 5-FU was found to form only wobble base pairs with guanine even under basic conditions (pH 9) in the crystal lattice.[13] This is a very surprising result because at pH 9 a significant portion of the molecule in solution should exist in the ionized form, which can pair with guanine by using two H-bonds, in the well-known Watson−Crick geometry.[13] Such changes in the stacking geometry could be connected with the mutagenic action of 5-FU. Furthermore, the specificity of the hydrogen bonding plays a central role in the transmission of genetic information, in the production of messenger RNA as well as in the polymerization of amino acids to form proteins. Thus, there is considerable interest in possible conformational changes with the pH value or environment and in the way 5-FU molecules associate.

SCHEME 1: Structure of Uracil (R = H) and Its 5-Halogenouracil Compounds (R = F, Cl, Br, I)

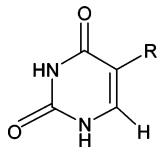

Recent Raman or SERS studies on 5-FU tried to analyze and detect the chemotherapy drug and its metabolites (e.g., 5-fluorouridine and 5-fluoro-2′-deoxyuridine) in saliva and blood by using metal-doped sol−gels[14,15] or to quantify its concentration and spatial distribution in some resorbable ocular solid implants.[16] However, they were never concerned with establishing and investigating its possible resonance structures and tautomers with the environment. Therefore, to identify and investigate for the first time the 5-FU species present at different pH values in water solution and near a biological artificial model (an Ag colloid), its Raman and SERS spectra at different pH values were recorded and discussed with the help of the DFT (density functional theory) calculations results. Here it is also taken into account that the experimental research and development in recent years have demonstrated SERS to be a potential technique for environmental and biological trace analysis, enabling the detection of even single molecules.[17] Moreover, SERS spectroscopy can provide information about the changes of molecular identity or orientation to the metal surface with the pH value.[18,19]

* To whom correspondence should be addressed. E-mail: ipavel@chem.ucsb.edu. Phone: 1-805-893-4070. Fax: 1-805-893-4075.
† Universität Würzburg.
‡ University of California at Santa Barbara.
§ Babeş-Bolyai University.

10.1021/jp053626q CCC: $30.25
Published on Web 10/14/2005

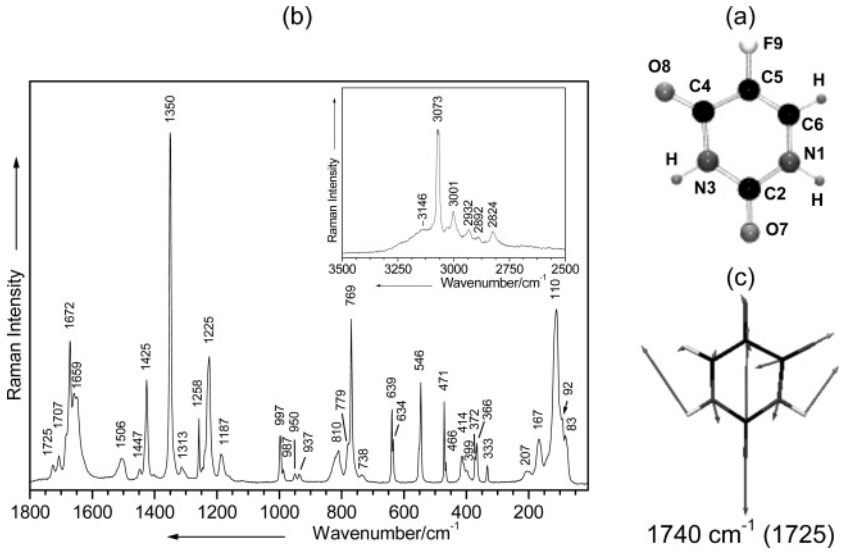

Figure 1. (a) B3LYP/6-311+G(d) optimized geometry of 5-FU; (b) FT-Raman spectrum of neat solid 5-FU (excitation line: $\lambda_0 = 1064$ nm); and (c) B3LYP/6-311+G(d) calculated vibrational mode of 5-FU, which implies C═O stretching vibrations and N−H deformation. The experimental Raman value is given in parentheses.

Overall, the results will provide a benchmark illustration of the virtues of DFT in aiding the interpretation of rich vibrational spectra attainable for such anticarcinogenic species by using Raman and SERS, as well as in furnishing detailed insight into the relation between the vibrational properties and the nature of the Ag substrate−adsorbate bonding at different pH values.

2. Experimental Section

2.1. Chemicals and Procedure. All starting materials involved in the preparation of the substrate and solutions were purchased from commercial sources as analytical pure reagents.

For the pH dependent Raman study, 5-FU aqueous solutions at different pH values were prepared by adding HCl or NaOH solutions (10^{-1} mol L^{-1}).

A sodium citrate-reduced Ag colloid was employed as SERS substrate. The yellowish sol was prepared according to the literature.[20,21] It presented a single extinction band at 408 nm. 5-FU aqueous solution (0.33 mL, 10^{-2} mol L^{-1}) was then added to 3 mL of colloid. The final 5-FU concentration in the SERS samples was about 10^{-3} mol L^{-1}. NaCl (40 μL of 0.5 M solution) was also added to produce a stabilization of the colloidal dispersion and a considerable enhancement of the SERS spectrum.[22] The pH values of the resulting mixtures were again adjusted with HCl or NaOH solutions.

2.2. Instrumentation. The FT-Raman spectrum of solid 5-FU was measured with a Bruker IFS 120-HR spectrometer equipped with an integrated FRA 106 Raman module. To avoid the fluorescence background, the radiation of 1064 nm from a Nd: YAG laser was employed for excitation with an output of 800 mW. A Ge detector was used and cooling was accomplished with liquid nitrogen. The spectral data were analyzed by using the OPUS 2.0.5 software. The spectral resolution was 1 cm^{-1}.

The micro-Raman and SERS spectra of 5-FU in the visible wavelength region were recorded with a Dilor Labram-Raman spectrometer equipped with 1800 grooves/mm holographic gratings. The 514.5 nm output of a Spectra Physics argon ion laser (Spectra Physics, Model 2016) was used to collect the spectra in the backscattering geometry with the help of a microscope featuring an Olympus LMPlanFL 50x objective. The laser output was set to 200 and 150 mW for the micro-Raman and SERS measurements, respectively. A Peltier CCD camera detection system and the analyzing software package LabSpec were employed for the data acquisition. The spectral resolution was in this case 3 cm^{-1}.

2.3. Computational Details. The ab initio and DFT calculations were performed with Gaussian 98.[23] Becke's three-parameter exchange functional (B3)[24] with Perdew and Wang's gradient-corrected correlation functional (PW91)[25,26] as well as Becke's three-parameter hybrid exchange functional (B3)[24,27] using the LYP correlational functional of Lee, Yang, and Parr (LYP)[28] were employed in the DFT calculations. The ab initio calculations were carried out by using the Hartree−Fock (HF) and the second order of Moller−Plesset (MP2) methods.[29,30] The 6-311+G(d) Pople split valence basis set and the LANL2DZ basis set implemented in the Gaussian 98 program[23] were chosen in the geometry optimization and normal modes calculations. The LANL2DZ basis set[31] was chosen with the intention to continue the calculations at the same level of theory for the Ag-adsorbed species of 5-FU.

The ab initio and DFT calculations on harmonic vibrational modes were performed by using fully optimized molecular geometry. The analytical harmonic vibrational wavenumbers for all structures confirmed that local minima on the potential energy surface had been found. The B3LYP/6-311+G(d), B3PW91/6-311+G(d), and HF/6-311+G(d) calculations were then continued to obtain the Raman scattering activity of each band.

The total electron density of the molecule (in e/au^3; au = atomic units) and the partial charges (in e) situated on selected atoms of 5-FU (by the natural population analysis (NPA)[32]) were determined at the above-mentioned level of theories. The total electron density was then plotted with the OpenMol package.[33]

3. Results and Discussion

3.1. Geometry Optimization. The optimized structural parameters of FU, calculated by using ab initio and DFT methods, are listed in Table 1S and the labeling of the atoms is shown in Figure 1a. The experimental data obtained by X-ray[34] diffraction studies on 5-FU are also included, to assess the accuracy of the geometry optimizations.

To obtain good starting geometries, the initial configurations were optimized at the HF and MP2 level of theory. The hybrid HF-DFT methods (B3LYP and B3PW91) were used on the optimized geometries obtained from ab initio calculations. As one can notice, the calculated bond distances and bond angles

SCHEME 2: Possible Tautomeric Forms of 5-FU

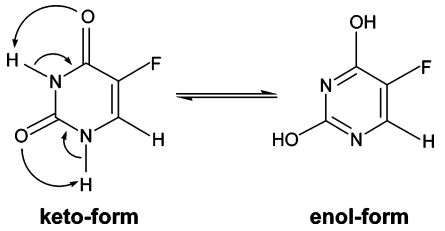

SCHEME 3: Protonation Reaction of 5-FU

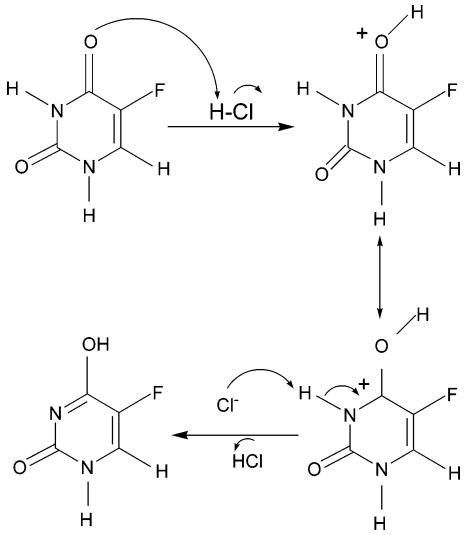

of 5-FU are very close to the reported parameters. The theoretical methods agree quite well with each other, but the bond lengths and angles of 5-FU were better reproduced in almost all cases by the B3LYP/6-311+G(d) method, where the maximum discrepancy was only 3 pm and 2.5° with respect to the experimental data. However, if one calculates the regression coefficients for the bond lengths and angles of 5-FU, MP2 leads to better results. DFT methods include electron correlation in a form that does not lead to the scaling problem of Hartree−Fock and MP2 based methods, and can lead to very accurate vibrational wavenumbers. But the higher accuracy comes at a higher cost in terms of CPU time. Therefore, DFT methods sustained by an extremely good ratio of CPU time/accurate calculation of the spectrum are preferable in such cases when a detailed vibrational analysis is required.

As expected, the ring is planar with the C−N and C−C single bond lengths, which have values between those observed in aromatic and saturated compounds. The fluorine atom at the 5th position was found to have a very small effect on the molecular structure, since the adjacent bond distances and bond angles do not differ from those measured in uracil very much.

Afterward, the keto- and enol-forms of 5-FU (Scheme 2) were analyzed for the first time at the same level of theories. The DFT calculation results helped us to establish the most stable resonance structure for each of those tautomers (Schemes 3 and 4) and interpret the Raman and SERS spectra at different pH values. The optimized structures are discussed later, in the Vibrational Spectroscopy section.

3.2. Vibrational Spectroscopy. *3.2.1. FT-Raman Spectrum.* For a correct interpretation of the SERS data it was necessary to have a complete assignment of the Raman spectrum. Theoretical calculations have aided the interpretation and many previously incomplete or incorrect assignments were analyzed and improved.

SCHEME 4: Deprotonation Reaction of 5-FU

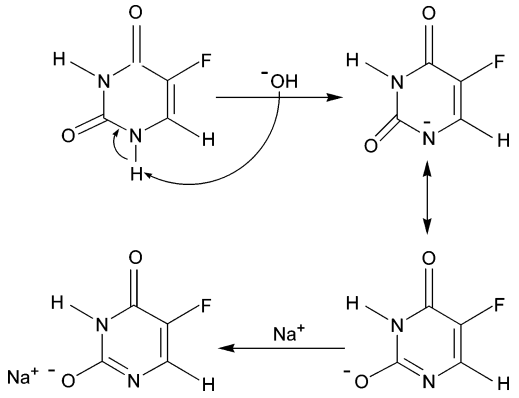

The FT-Raman spectrum of 5-FU recorded in the 3600−150 cm^{-1} spectral region is presented in Figure 1b. The observed bands along with their assignments are summarized in Table 2. The vibrational fundamentals from the Raman spectrum were analyzed by comparing them with those assigned in the literature[35−37] in conjunction with theoretical calculations.

Ab initio harmonic vibrational wavenumbers are typically larger than the observed fundamentals (Table 2).[29] After proper scaling,[24,27] the HF calculated modes come closer to the experimental values, but not closer than the DFT results. As one can notice, the vibrational assignment in the experimental spectrum was feasible with the help of the DFT calculations (Table 2). But consistent with previous findings,[38,39] the B3LYP and B3PW91 functionals tend to overestimate some fundamental modes. This disagreement of about 5% may be due partly to the anharmonicity and partly to the general tendency of most quantum chemical methods to overestimate force constants at the exact equilibrium geometry. Particularly, vibrations involving central atoms with lone pairs (such as the N1 and N3 atoms) and the CH vibrations for which anharmonicity is large show significant deviations. After proper scaling,[40] the B3LYP computed wavenumbers, which presented larger deviations, were in good agreement with the experimental modes. However, one should take into account that the calculations on 5-FU refer to the gas phase and not to the solid state, which implies the existence of H-bonding mainly between the C═O and N3−H groups. This could also explain the significant deviations for some of the calculated wavenumbers and Raman scattering activities, especially those involved in hydrogen bonds. Here it should be taken into account that the intermolecular forces (hydrogen bonds) present in the solid state play a dominant role in the position and intensity of IR and Raman modes.

The molecule belongs to the C_s point group with the following normal mode distribution: $21a' + 9a''$. Out of these 30 characteristic vibrational modes we will only discuss the ones presenting a very interesting or complex spectral pattern.

The first region showing a complex pattern is that of the N−H stretching modes. As one can notice, it consists of two weak bands located at 3146 and 3001 cm^{-1}, which were attributed to the N1−H and N3−H stretching modes. It must be mentioned that the N3−H group is mainly involved in C═O···H−N bonds. The peak at 3073 cm^{-1} (B3LYP/6-311+G(d) calculated, 3104 cm^{-1}) presenting the highest intensity among the bands in the 3000 cm^{-1} spectral region was assigned to the C6−H stretching mode, because the hydrogen atom at the C6 position is not involved in any hydrogen bonds and therefore it should be the most intense peak in this region (Figure 1b).

The typical pattern of the C═O stretching region (here represented by four peaks at 1725, 1707, 1672, and 1659 cm^{-1})

TABLE 2: Selected Calculated and Experimental Raman and SERS Wavenumbers (cm^{-1}), along with Their Tentative Assignments[a]

	calcd B3LYP/6-311+G(d)			HF/6-311+G(d)		
FT-Raman solid state		scale[b]	B3PW91/6-311+G(d)		scale[c]	vibrational assignment
3146 sh	3644 (93.54)	3509	3665 (89.86)	3907 (75.20)	3513	ν(N1−H)
3073 w	3223 (105.90)	3104	3231 (103.43)	3404 (83.91)	3061	ν(C6−H)
3001 vw	3600 (68.59)	3467	3620 (66.47)	3864 (52.78)	3475	ν(N3−H)
2932 vw						1707 + 1225
2892 vw						2 × 1447
2824 vw						1350 + 2 × 738
1725 vw	1807 (29.40)	1740	1831 (27.78)	1986 (63.40)	1786	FR between ν(C2═O7) + ν(C4═O8) + δ
1707 vw						(N−H) at 1715 and 1718 = 950 + 768
1672 m	1780 (59.74)	1714	1803 (58.16)	1968 (12.99)	1770	ν(C4═O8) + ν(C2═O7) + δ(N−H)
1659 w	1714 (44.45)	1651	1729 (44.52)	1901 (77.55)	1709	ν(C5═C6)
1506 vw	1508 (8.72)		1520 (7.71)	1654 (7.03)	1487	δ(N1−H) + ν(ring)
1447 vw						810 + 639
1425 w	1431 (4.12)		1441 (2.08)	1575 (4.78)	1416	δ(N−H) + ν(ring)
1350 vs	1418 (2.21)	1365	1422 (2.08)	1562 (2.81)	1405	δ(N−H) + ν(ring)
1313 vw						769 + 546
1258 w	1351 (30.11)	1301	1357 (30.45)	1484 (40.11)	1334	δ(C6−H) + ν(ring) + δ(N1−H)
1225 m	1255 (4.59)	1209	1277 (4.60)	1368 (7.52)	1230	ν(C5−F9) + δ(N1−H) + ν(ring)
1187 vw	1184 (2.68)		1198 (2.68)	1313 (2.22)	1181	δ(N3−H) + δ(C6−H) + ν(ring)
997 vw	1155 (4.24)	1112	1169 (2.68)	1244 (1.47)	1119	δ(N−H) + δ(C6−H) + ν(ring)
987 vw						2 × 110 + 769
950 vw	970 (2.23)	934	978 (2.18)	1055 (1.67)	949	δ(C6−H) + δ(N3−H) + δ(ring)
937 vw	891 (2.27)		890 (2.16)	1028 (4.58)	924	γ(C6−H)
810 vw	815 (4.84)		819 (4.60)	891 (2.19)	801	δ(ring)
779 sh	762 (1.32)		766 (1.32)	845 (3.32)	760	γ(C4═O8) + γ(N3−H) + γ(ring)
769 m	754 (0.01)		760 (0.01)	853 (0.55)	767	γ(C2═O7) + γ(N3−H) + γ(ring)
738 vw	740 (15.60)		747 (15.74)	792 (10.56)	720	δ(ring)
639 w	669 (0.97)	644	675 (0.96)	711 (1.05)	646	γ(N3−H) + γ(ring)
634 vw	630 (5.37)		632 (5.33)	688 (4.96)	625	δ(ring)
546 w	542 (0.12)		549 (0.13)	549 (0.05)		γ(N1−H)
471 w	537 (5.23)	517	538 (5.10)	586 (3.72)	533	δ(ring) (δ(N−H) + δ(C═O) + δ(C6−H))
466 sh	456 (3.75)		456 (3.54)	491 (2.49)	446	δ(ring) (δ(C5−F9) + δ(C═O) + δ(N−H))
414 vw	389 (1.65)		391 (1.61)	431 (1.20)		δ(ring) (δ(OCNCO))
399 sh						333 + 68
372 vw						207 + 167
366 vw	378 (1.23)	364	378 (1.19)	409 (2.51)	372	γ(ring) (γ(C6−H) + γ(N−H))
333 vw	341 (0.48)	328	345 (0.46)	370 (0.26)	336	γ(ring) (γ(C5−F9) + γ(C6−H) + γ(N1−H))
207 vw	304 (0.34)	293	303 (0.35)	330 (0.33)	300	δ(OCCF)
167 vw	151 (0.01)		151 (0.01)	159 (0.01)		γ(ring) (γ(C═O) + γ(N−H))
110 ms	114 (0.44)	110	115 (0.43)	118 (0.35)	107	γ(ring) (γ(C═O) + γ((C5−F9) +
						γ(N1−H) + γ(C6−H))
92 sh						lattice modes
83 sh						
68 sh						

[a] Abbreviations: vw, very weak; w, weak; m, medium; ms, medium strong; s, strong; vs, very strong; sh, shoulder; ν, stretching, δ, in-plane deformation; γ, out-of-plane deformation; FR, Fermi resonance. The calculated Raman scattering activities in parentheses are in $Å^4$/amu. [b] Scaled by 0.963 according to the value proposed by Rauhut and Pulay.[40] [c] Scaled by 0.8992 (above 800 cm^{-1}) and 0.9089 (below 800 cm^{-1}) according to the values proposed by Becke.[24,27]

is very complex. One of the two characteristic C═O modes is split into two components at 1725 and 1707 cm^{-1} due to the Fermi resonance of the fundamentals with combination bands (Table 2). Also, the fluorine atom has a great influence on the ν(C═O) modes. The halogen effect on the C2═O7 and C4═O8 stretching mode positions is stronger on the C4═O8 group, which is located closer to the fluorine atom. The inductive effect of the electronegative halogen would tend to diminish the charge density on the carbon atom, which is the nearest to the halogen atom. Accordingly, the ν(C2═O7) should be ascribed at higher wavenumbers, namely at 1725 cm^{-1}, whereas the ν(C4═O8) should be ascribed at lower ones (1672 cm^{-1}). Nevertheless, the oxygen atom at the C4 position is involved in hydrogen bonding and thus the ν(C4═O8) mode should have a smaller relative intensity, which is contrary to the experimental data. It seems that the halogen influence on the C4═O8 bond overcomes the intermolecular hydrogen bonding effects. In good agreement with Rastogi et al.'s work,[35] our calculation results indicate a slight mixing of the two carbonyl stretching modes for each of the mentioned bands (e.g., the C2═O7 (≈80%) and C4═O8 (≈10%) stretching modes mix to give rise to the peak at 1725 cm^{-1}). The DFT calculations suggest a C5═C6 stretching vibration for the last peak at 1659 cm^{-1}, which was also found to be very sensitive to the nature of the X-substituent.[36,37]

It must be mentioned that some differences in assignment (regarding Rastogi et al.'s results for 5-FU) were noticed for the out-of-plane deformation modes of the C═O groups (779 and 769 cm^{-1}). Because of the involvement of the O atom at the C4 position in hydrogen bonding, both the planar and the nonplanar deformations of the C4═O8 bond are more obstructed than the corresponding movements of the C2═O7 bond. Therefore, the γ(C2═O7) mode should have a higher relative intensity than the γ(C4═O8). Accordingly, the shoulder at 779 cm^{-1} was attributed to the γ(C4═O8) mode, while the peak of medium intensity at 769 cm^{-1} was ascribed to the γ(C2═O7) vibration. However, Rastogi et al. proposed an opposite trend and attributed the peak at 810 cm^{-1} of very weak relative intensity to the γ(C2═O7) mode (our DFT results indicated a

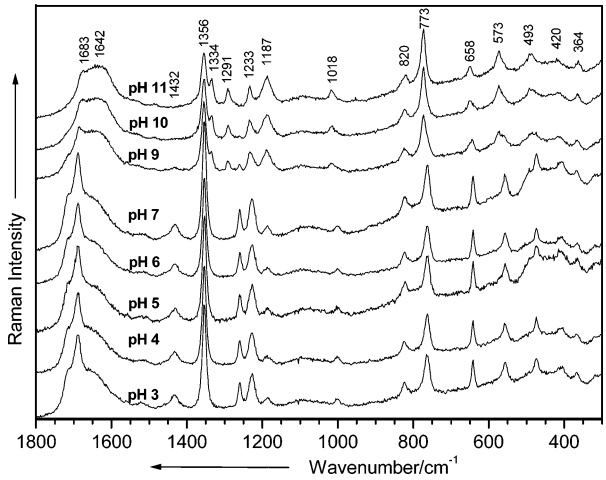

Figure 2. Micro-Raman spectra of the 5-FU water solution (10^{-1} mol L^{-1}) at different pH values. Excitation line: $\lambda_0 = 514.5$ nm.

ring deformation for this peak), whereas the signal at 769 cm^{-1}, of a much higher intensity, was considered to be due to the γ(C4═O8) vibration (Table 4 in ref 35).

The most intense band observed in this spectrum is that at 1350 cm^{-1} (B3LYP/6-311+G(d) calculated, 1365 cm^{-1}), which was assigned to a ring stretching mode that plays a very important role in the SERS behavior analysis.

The C5−F9 stretching mode appears at 1225 cm^{-1} as a medium intense peak. The B3LYP/6-311+G(d) calculations place the δ(C5−F9) and γ(C5−F9) modes at 456 and 328 cm^{-1}. Accordingly, the observed bands at 414 and 333 cm^{-1} were assigned to the δ(C5−F9) and γ(C5−F9) modes, respectively.

3.2.2. Micro-Raman Spectra of 5-FU Solution (10^{-1} mol L^{-1}) at Different pH Values. It is well-known that most carbonyl compounds exist almost exclusively in their keto form at equilibrium and it is usually difficult to isolate the pure enol. Now, let us take a closer look at the micro-Raman spectra of the 5-FU solution to see whether we can identify the two above-mentioned species (Figure 2).

Both acids and bases catalyze the keto−enol tautomerism (Scheme 2).

The protonation of the carbonyl bond occurs at acid pH values. The oxygen atom acts as a Lewis base taking the H-atom from the chloric acid and regenerating an intermediate cation that can be represented by two resonance forms. The most stable intermediate cation loses its proton and leads to the enol form (Scheme 3). The geometry optimization of the two enol forms performed at the B3LYP/6-311+G(d) level showed that the species protonated at O7 are more stable than the ones protonated at the O8 atom. This may be due to a larger dislocation of the negative charge on the first compound. The absolute energy difference, ΔE_0, between the two species is not large, about 6.18 kJ/mol, and contains the zero-point energy (ZPE) correction. Other thermochemical properties, like the entropy (S), the enthalpy ($H = E + RT$), and the Gibbs free energy ($G = H - TS$) have also been evaluated. All of them include ZPE.

The relative conformer or tautomer abundances can be computed by using $\Delta G = -RT \ln K_C$, where ΔG is the difference in Gibbs energy and K_C is the concentration ratio of the investigated forms. These new calculations seem to qualitatively favor the same conformers/tautomers as the initial ones. However, the molecular modeling of a single structure does not include any intermolecular interactions and thus it is the equivalent to predicting the monomeric structure in the vapor phase. In solution the structure is surrounded by solvent molecules and as a neat liquid it is surrounded by other similar structures. Further calculations regarding the solvent effects (by placing the analyte in a dielectric continuum of the bulk solvent and by the explicit addition of water molecules) are in progress. These might predict and describe better the change in the energy difference between the different tautomeric forms in a polar solvent like H_2O.

The presence of the in-plane and out-of-plane N3−H deformation modes at 1187 and 658 cm^{-1} seems to confirm this conclusion (in FT-Raman detected at 1187 and 639 cm^{-1}, respectively). The first enol form may also be present at these pH values, but in a very low concentration. This is due to the fact that the in-plane and out-of-plane deformation modes of the N1−H group (1506 and 546 cm^{-1} in FT-Raman) are either absent or weaker in the micro-Raman spectrum of the solution (Figure 2).

Moreover, the carbonyl spectral region is dominated by a very strong peak at about 1689 cm^{-1}, which is due to the ν(C4═O8) mode. Because of the protonation at the O7 atom, the C2═O7 stretching is more obstructed than the corresponding motion of the C4═O8 bond, and consequently, it should have a much lower intensity. Indeed, the ν(C2═O7) mode appears in the SERS spectra at acid pH values as a weaker shoulder at higher wavenumbers.

At basic pH values, the base (in our case the hydroxyl group) deprotonates the N1−H bond, leading to an intermediate anion—an enolate ion—that could be again represented by two resonance structures (Scheme 4).

The Na^+ addition to the oxygen atom will yield the neutral enolate. The geometry optimization of the two deprotonated forms indicated the form deprotonated at the N1 atom as being the most stable one by 12.57 kJ/mol. This energy difference could be explained by the fact that the deprotonation at the N3 atom occurs very quickly and leads to a kinetically controlled product, while the deprotonation at the N1 atom occurs slowly leading to a thermodynamically controlled product. The micro-Raman spectra allowed us once more to experimentally distinguish between these two enolate forms (Figure 2).

The C5−F9 stretching and the ring stretching modes at 1233 and 1258 cm^{-1}, which are strongly coupled with the N1−H deformation mode, decrease significantly in intensity or disappear on passing from acid to basic pH values. The N3−H bending mode at 1187 cm^{-1} presents a reverse behavior. Moreover, two new signals were detected at 1334 and 1291 cm^{-1} and assigned to simultaneous vibrations of the N3−H moiety and the ring.

The band at 1432 cm^{-1} (in FT-Raman detected at 1425 cm^{-1}), which mainly results from a N1−H bending mode slightly coupled with a N3−H deformation and a ring stretching, decreases very much in intensity with the increase in the pH value.

Even CO stretching modes at these pH values are not well resolved: their shift to smaller wavenumbers and decrease in relative intensity confirm the Na^+ addition at the oxygen atom.

The ν(C4═O8) mode at 1683 cm^{-1} suffers the most evident changes, due to the possibility of forming hydrogen bonds with the water molecules present in solution. These seem to indicate the enolate form deprotonated at N1 as being the most stable one but does not exclude the presence of the other form deprotonated at the N3 atom in a very small concentration.

3.2.3. SERS Spectra of 5-FU on Ag Colloid at Neutral and Basic pH Values. A closer examination of the normal Raman and SERS spectra of 5-FU on Ag sol at neutral and basic pH

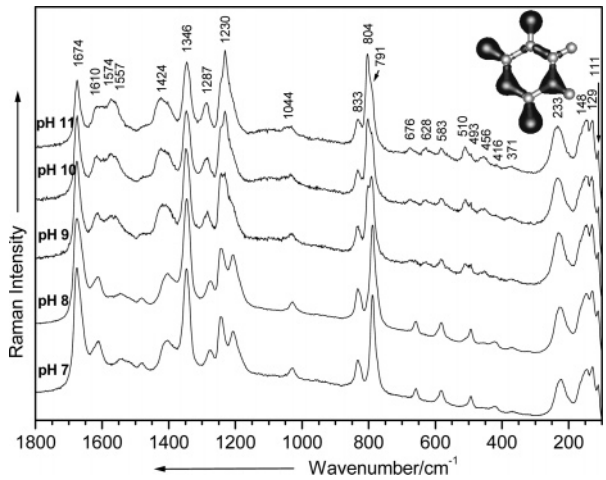

Figure 3. SERS spectra of 5-FU on Ag colloid at neutral and basic pH values. Excitation line: $\lambda_0 = 514.5$ nm. The total electron density of the N3-deprotonated form of 5-FU is inserted (isosurface value: 0.27).

values (Figures 2 and 3) shows major differences in band positions and their relative intensities, which indicates a very strong interaction of the sample with the Ag surface.

The DFT calculations performed at the B3LYP/LANL2DZ level helped us to identify the most stable tautomers and Ag-complexes. We observed that the N1-deprotonated form is more stable than the N3 one, but for the Ag-complexes the energy levels are reversed, more precisely, the second tautomer becomes more stable. This might be due to a smaller delocalization of the negative charge and to a higher dipol moment for the N3 deprotonated form.

Almost all bands present in the SERS spectrum at neutral pH can also be detected at basic pH values. This fact demonstrates that 5-FU is adsorbed to the Ag surface in its deprotonated form even at neutral pH (Figure 3). At basic pH values, some of the peaks that were present at neutral pH disappear and some new ones emerge. The most likely explanation for the additional bands at high pH is the coexistence of both deprotonated forms. However, as we will show below, one of the tautomers seems to prevail at these pH values.

The SERS spectra at alkaline pH values are dominated by the peaks at 1674, 1346, 1230, and 804 cm^{-1}. The most significant changes are to be seen for the bands at 1674 and 1230 cm^{-1}, which present a significant enhancement in comparison with their relative intensities in the micro-Raman spectra of the 5-FU solution at the same pH values (Figures 2 and 3).

The peak at 1230 cm^{-1} corresponds to the C5−F9 stretching vibration strongly coupled with an N1−H deformation, which indicates the strong presence of the N3-deprotonated form. This is further confirmed by the broad band at 1424 cm^{-1}, which is mostly due to a N1−H bending mode slightly coupled with an N3−H deformation and a ring stretching. As one can notice, it has a much higher intensity than in the micro-Raman spectra at the same pH values. However, the presence of the second N1-deprotonated form at high pH values cannot be excluded because the in-plane deformation mode of the N3−H group also appears in the SERS spectra as a weak red shoulder for the very strong signal at 1230 cm^{-1}. Furthermore, moving toward neutral pH values, the shoulder develops into a clear peak of medium relative intensity (1208 cm^{-1} at pH 7), indicating a considerable increase in concentration of the second N1-deprotonated form.

The very strong bands at 1674 and 804 cm^{-1} are mainly due to the C4═O8 stretching and out-of-plane deformation modes, respectively. Taking into account that at these pH values, the N3-deprotonated form seems to dominate, a strong adsorption probably through the O7 atom in a perpendicular orientation to the surface or an orientation not significantly tilted from the surface normal would explain the observed enhancement. The perpendicular or the tilted orientation is further substantiated by the very strong ring stretching mode at 1350 cm^{-1}. According to the SERS surface selection rules, this vibration should be the most prominent band in the SERS spectrum, when the molecule stands upright on the surface. Moreover, as we already mentioned, the C5−F9 stretching mode at 1230 cm^{-1} is one of the dominant bands in the SERS spectra at alkaline pH values. A chemisorption through the O7 atom in a perpendicular orientation or not significantly tilted from the surface normal would lead to a significant increase in relative intensity of this mode, as was observed.

However, in most of the cases, precise determination of the adsorption site on the Ag surface is fraught with problems. From the chemical structure, one can observe (Scheme 4) that the deprotonated forms of 5-FU have three atoms, namely the two O atoms and one of the N atoms, capable of forming bonds with the silver surface, while in the protonated forms both N atoms and one O atom are available (Scheme 3). The best way of treating this problem is to enumerate the negative charge density on each of these possible active sites. The higher the negative charge density on the atom, the higher is its probability to act as an adsorptive site for the Ag substrate.

The representative plot of the total electron density for the N3-deprotonated form (inserted in Figure 3) indicates a build-up of charge density on the fluorine (only slightly charged), oxygen, and nitrogen atoms, as well as nodes at the other atoms. The DFT calculations at the B3LYP/6-311+G(d) and B3PW91/6-311+G(d) levels of theory (Table 3S) led to very similar values in the deprotonated and protonated forms of 5-FU. The highest negative charge densities for the dominant N3-deprotonated tautomer were found on the oxygen atoms, i.e., of −0.732 and of −0.685 (e) on the O7 and O8 atoms, respectively, by using the B3LYP functional. As expected, the C2═O7 carbonyl group is a little more basic than the C4═O8 carbonyl group, since the C2═O7 carbonyl group is joined to two N atoms, while the C4═O8 carbonyl group is joined to one N atom and to an sp^2 carbon atom. One can notice that the negative charge density on the N3 atom is also great, being very close to the one on the O8 atom. Therefore, it is likely that all three atoms (i.e., O7, O8, and N3) can be active sites for the adsorption process, but the O7 atom has a little higher probability. This might confirm our supposition regarding the O7 atom acting as an adsorptive site at the Ag surface.

To gain more information about possible adsorptive sites for the Ag substrate, the spectral region around 200 cm^{-1} has been examined closer, since the Ag−O and Ag−N stretching modes are generally observed in this low wavenumber spectral region. The SERS spectra of 5-FU at alkaline and neutral pH values present a strong broad band at about 233 cm^{-1} (Figure 3), which can be due to the Ag−O stretching mode. This may indicate a bonding with the Ag surface through the lone pairs of the O7 atom.

At neutral pH values, a new band appears at 1277 cm^{-1} as a result of some in-plane vibrations, more exactly due to a C6H bending coupled with a N3C4 stretching and a N1H bending mode. This new signal might result from an adsorption of the N3-deprotonated form through its O7 or N3 atom. According to the SERS surface selection rules, a perpendicular orientation of the molecule on the Ag surface or an orientation not

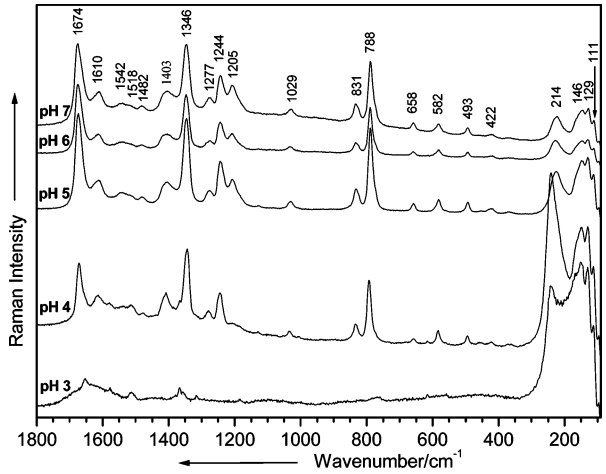

Figure 4. SERS spectra of 5-FU on Ag colloid at neutral and acid pH values. Excitation line: $\lambda_0 = 514.5$ nm.

significantly tilted from the surface normal would greatly enhance the N3C4 stretching if the interaction atom is O7. If the adsorption takes place through the N3 atom, the C6−H bending will have a large Raman polarizability component perpendicular to the surface and should exhibit a significant increase in intensity. However, it must be mentioned that this band mainly arises from a C6H bending (65%),[35] which shows that the adsorption through the N3 atoms cannot be excluded. The signal shifts to even higher wavenumbers with the increase in the pH value confirming the increase in concentration for the N3-deprotonated adsorbed species.

Therefore, at neutral and basic pH values, the SERS surface selection rules in combination with the DFT results indicate a chemisoption of both enolate forms. It seems that at alkaline pH, both deprotonated forms of 5-FU are present in the solution and both tautomers adsorb on the Ag surface in a perpendicular orientation or an orientation not significantly tilted from the surface normal. However, the N3 deprotonated form seems to be the dominant tautomer in the adsorbed state, more probably attached through the O7 atom to the metal surface.

3.2.4. SERS Spectra of 5-FU on Ag Colloid at Neutral and Acid pH Values. The SERS spectra of 5-FU on Ag colloid at acid and neutral pH values are represented in Figure 4.

Most of the bands observed at neutral pH are also present at smaller pH, providing evidence that 5-FU might be adsorbed to the Ag surface in its deprotonated forms even at acid pH. The pK_a value for the deprotonation at the N atom seems to be changed in the presence of the Ag colloid to generate the enolate forms even at acid pH values. This can replace the citrate ions and interact with the positively charged Ag surface via the negatively charged N atom or the lone pair of the oxygen atoms. The positive charges on the colloidal surface seem to lower the pK_a value of 5-FU by the Coulombic stabilization of the deprotonated anion. It would be of interest in this regard to exactly determine the change in the pK_a of the 5-FU SERS final solutions with the pH value. Further investigations are in progress.

As one can notice, only a few peaks seem to disappear or change their profile in the SERS spectra at these pH values. This might indicate a slight change in the concentration of one of the two tautomeric forms. More exactly, the band at 1205 cm^{-1}, which corresponds to the N3H bending mode, disappears at smaller pH values. Therefore, the concentration of the N3-deprotonated form might increase at more acid pH values. This observation is completed by the out-of-plane N3H deformation mode at 658 cm^{-1}, whose relative intensity drops in the SERS spectra in comparison with the micro-Raman spectra at the same pH values. Moreover, the broad band at 1403 cm^{-1} (pH 7), which mainly results from a N1−H bending mode slightly coupled with a N3−H deformation and a ring stretching, increases in intensity with the decrease in the pH value. All this indicates the N3-deprotaned tautomer as being the dominant form in these conditions.

At acid pH values, three very strong bands were observed in the SERS spectra, namely at 1672, 1344, and 789 cm^{-1}. The ring stretching mode at 1344 cm^{-1} is again a clear indication for the upright orientation of the molecule on the Ag surface. The other two peaks at 1672 and 789 cm^{-1} correspond to the C4═O8 stretching and out-of-plane deformation modes. According to the SERS surface selection rules, the carbonyl group should be close to the Ag surface and should have a large Raman polarizability component perpendicular to the surface in order to present such an enhancement. The chemisorption through the N3 or O7 atom would obviously lead to such spectral changes. This is further supported by the calculated negative charge densities on the nitrogen and oxygen atoms in the N3-deprotonated form (Table 3S) and the possible Ag−O or Ag−N stretching mode observed at about 214 cm^{-1} in the SERS spectra at pH 7, 6, and 5.

A closer examination of the SERS spectra at pH 3 and 4 shows a very strong increase in relative intensity in the 300−100 cm^{-1} spectral region. The very strong band at 241 cm^{-1} is most likely a Ag−Cl stretching mode (pH 4), because its relative intensity increases with the increase in the Cl^- concentration. Therefore, at pH 3 and 4, we cannot make any comments regarding the silver−nitrogen or silver−oxygen interaction (i.e., the ν(Ag−N) or ν(Ag−O) modes), which may be here hidden under the Ag−Cl band.

The intensity of the signals drops at more acid values (below pH 4) and good resolved peaks are difficult to observe.

In conclusion, at acid pH values, the molecule was found to be chemisorbed on the metal surface through the N3 or O7 atoms of the N3-deprotonated form, more probably through the lone pair of the O7 atom in an end-on orientation.

4. Conclusions

The normal Raman and SERS spectra of 5-fluorouracil were recorded and discussed with the help of the DFT calculations results. The combination of these two approaches (i.e., theoretical and experimental) proved to be a very powerful tool not only for establishing and detecting the very important biological species of 5-FU for the first time, but also to correctly discriminate between them in water solution and as adsorbed species at different pH values. This combination has a rapid response time with little sample preparation needed for the collection of data. Together with the uniqueness of the spectra, these attributes make this method a viable candidate for inclusion in a rapid, sensitive biological method of detecting and studying such essential anticarcinogenic species or biological threats in different conditions.

We strongly believe that theoretical calculations will become a matter of rapidly growing scientific and practical interest in SERS. Currently we try to model the adsorption of very simple molecules on an Ag substrate by the construction of an "ideal" cluster and by using different theoretical approaches. The challenge here is how to treat the interaction of an electronically localized system like a 5-FU molecule with an electronically delocalized structure such as a metal particle. Regarding this aspect very few results have been reported so far and almost all have involved only a single or too few metal atoms (including

the present one). These studies clearly do not provide a quantitative model of the metal surface.[41−43] However, there has been recent progress in the use of computational electrodynamics methods including the discrete dipole approximation, the finite difference time domain method, and the electronic structure methods that explicitly include the electric fields from the classical electrodynamics calculation in the determination of Raman intensities to model such interactions.[43] Therefore, there are significant opportunities for improved work in this area.

Acknowledgment. We acknowledge the financial support from the Deutsche Forschungsgemeinschaft (Sonderforschungsbereich SFB 630, Teilprojekt C1), as well as that from the Fonds der Chemischen Industrie.

Supporting Information Available: Table 1 giving selected calculated structural parameters compared with the crystal structure data for 5-FU and Table 3 giving partial charges (in e) situated on selected atoms of 5-FU deprotonated and protonated forms, which were determined by Natural Population Analysis. This material is available free of charge via the Internet at http://pubs.acs.org.

References and Notes

(1) Goodman, L. A.; Gilman, A. In *The Pharmacological Basis of Therapeutics*, 6th ed.; Macmillan: New York; 1980.

(2) Heidelberg, C. In *Cancer Medicine*; Holland, J. F., Frei, E., III, Eds.; Lea & Febiger: Philadelphia, PA, 1982; p 801.

(3) Heidelberger, C.; Danenberg, P. V.; Moran, R. G. *Adv. Enzymol.* **1983**, *54*, 58−119.

(4) Valeriote, F.; Santelli, G. *Pharmacol. Ther.* **1984**, *24*, 107−132.

(5) Graham, M. A.; Lockwood, G. W.; Greenslade, D.; Brienza, S.; Bayssas, M.; Gamelin, E. *Clin. Cancer Res.* **2000**, *6*, 1205−1218.

(6) Martenson, J. A.; Lipsitz, S. R.; Wagner, H., Jr.; Kaplan, E. H.; Otteman, L. A.; Schuchter, L. M.; Mansour, E. G.; Talamonti, M. S.; Benson, A. B., 3rd *Int. J. Rad. Onc. Biol. Phys.* **1996**, *35*, 745−749.

(7) Goodman, L. A.; Gilman, A. In *The Pharmacological Basis of Therapeutics*, 9th ed., McGraw-Hill: New York, 1996; p 1247.

(8) Dorman, D. C.; Coddington, K. A.; Richardson, R. C. *J. Vet. Intern. Med.* **1990**, *4*, 254−257.

(9) *Basic and Clinical Pharmacology*, 6th ed.; Katzung, B., Ed.; Appleton & Lange Stanford, CT, 1995.

(10) Kim, H. O.; Ahn, S. K.; Alves, A. I.; Beach, I. W. *J. Med. Chem.* **1992**, *35*, 1987−1995.

(11) Verheggen, I.; Van Aerschot, A.; Van Meervelt, L.; Rozenski, J.; Wiebe, L.; Snoeck, R.; Andrei, G.; Balzarini, J.; Claes, P.; De Clercq, E. *J. Med. Chem.* **1995**, *38*, 826−835.

(12) Seela, F.; Muth, H.-P. *Liebigs Ann. Chem.* **1988**, *215*−*219*.

(13) Coll, M.; Saal, D.; Frederick, C. A.; Aymami, J.; Rich, A.; Wang, A. H.-J. *Nucleic. Acids Res.* **1989**, *17*, 911−923.

(14) Gift, A. D.; Shende, C. S.; Inscore, F. E.; Farquharson, S. *Proc. SPIE−Int. Soc. Opt. Eng.* **2004**, *5588* (Smart Medical and Biomedical Sensor Technology II), 70−77.

(15) Farquharson, S.; Maksymiuk, P. U S. Patent Appl. Publ. 2004, 12 pp.

(16) Milne, P.; Gautier, S.; Parel, J.-M.; Jallet, V. *Proc. SPIE−Int. Soc. Opt. Eng.* **1997**, *2971* (Ophthalmic Technologies VII), 137−146.

(17) Nie, S.; Emory, S. R. *Science* **1997**, *275*, 1102−1106.

(18) Suh, J. S.; Jang, N. H.; Jeong, D. H.; Moskovits, M. *J. Phys. Chem.* **1996**, *100*, 805−813.

(19) Moskovits, M.; Suh, J. S. *J. Phys. Chem.* **1984**, *88*, 1293−1298.

(20) Lee, P. C.; Meisel, D. P. J. *J. Phys. Chem.* **1982**, *86*, 3391−3395.

(21) Munro, C. H.; Smith, W. E.; Garner, M.; Clarkson, J.; White, P. C. *Langmuir* **1995**, *11*, 3712−3720.

(22) Brandt, E. S.; Cotton, T. M. *Physical Methods of Chemistry Series*, 2nd ed.; Wiley: New York, 1993; Vol. IXB.

(23) Frisch, M. J.; Trucks, G. W.; Schlegel, H. B.; Gill, P. M. W.; Johnson, B. G.; Robb, M. A.; Cheeseman, J. R.; Keith, T.; Petersson, G. A.; Montgomery, J. A.; Rhaghavachari, K.; Al-Laham, M. A.; Zakrzewski, V. G.; Ortiz, J. V.; Foresman, J. B.; Ciolowski, J.; Stefanov, B. B.; Nanayakkara, A.; Challacombe, M.; Peng, C. Y.; Ayala, P. Y.; Chen, W.; Wong, M. W.; Andres, J. L.; Replogle, E. S.; Gomberts, R.; Martin, R. L.; Fox, D. J.; Binkley, J. S.; Defrees, D. J.; Baker, J.; Stewart, J. P.; Head-Gordon, M.; Gonzalez, C.; Pople, J. A. *Gaussian 98*, Revision A7; Gaussian Inc.: Pittsburgh PA, 1998.

(24) Becke, A. D. *J. Chem. Phys.* **1993**, *98*, 5648−5652.

(25) Perdew, J. P. In *Electronic Structure of Solids*; Ziesche, P., Eschrig, H., Eds.; Akademie Verlag: Berlin, Germany, 1991.

(26) Perdew, J. P.; Wang, Y. *Phys. Rev. B* **1992**, *45*, 13244−13249.

(27) Becke, A. D. *J. Chem. Phys.* **1992**, *97*, 9173−9177.

(28) Lee, C.; Yang, W.; Parr, R. G. *Phys. Rev. B* **1988**, *37*, 785−789.

(29) Hehre, W. J.; Radom, L.; Schleyer, P. v. R.; Pople, J. A. In *Ab Initio Molecular Orbital Theory*; John Wiley & Sons: New York, 1986.

(30) Moller, C.; Plesset, M. S. *Phys. Rev.* **1934**, *46*, 618−622.

(31) Dunning, T. H.; Hay, P. J., Jr. In *Modern Theoretical Chemistry*; Schaefer, H. F., III, Ed.; Plenum: New York, 1976; pp 805−888.

(32) Reed, A. E.; Weinstock, R. B.; Weinhold, F. *J. Chem. Phys.* **1985**, *83*, 735−746.

(33) Laaksonen, L. http://laaksonen.csc.fi/gopenmol/gopenmol.html, Espoo: Finlannd.

(34) Fallon, L., III *Acta Crystallogr.* **1973**, *B29*, 2459−2556.

(35) Rastogi, V. K.; Jain, V.; Yadav, R. A.; Singh, C.; Palafox, M. A. *J. Raman Spectrosc.* **2000**, *31*, 595−603.

(36) Zwierzchowska, Z.; Dobrosz-Teperek, K.; Lewandowski, W.; Kolos, R.; Bajdor, K.; Dobrowolski, J. Cz.; Mazurek, A. P. *J. Mol. Struct.* **1997**, *410*−*411*, 415−420.

(37) Dobrosz-Teperek, K.; Zwierzchowska, Z.; Lewandowski, W.; Bajdor, K.; Dobrowolski, J. Cz.; Mazurek, A. P. *J. Mol. Struct.* **1998**, *471*, 115−125.

(38) Scott, A. P.; Radom, L. *J. Phys. Chem.* **1996**, *100*, 16502−16513.

(39) Santamaria, R.; Charro, E.; Zacarías, A.; Castro, M. *J. Comput. Chem.* **1999**, *20*, 511−530.

(40) Rauhut, G.; Pulay, P. *J. Phys. Chem.* **1995**, *99*, 3093−3100.

(41) Wu, D.-Y.; Duan, S.; Ren, B.; Tian, Z.-Q. *J. Raman Spectrosc.* **2005**, *36*, 533−540.

(42) Mrozek, M. F.; Wasileski, S. A.; Weaver, M. J. *J. Am. Chem. Soc.* **2001**, *123*, 12817−12825.

(43) Zhao, L.; Zou, S.; Hao, E.; Schatz, G. C. In *Theory and Applications of Computational Chemistry*: *The First Forty Years*, Dykstra, C., Frenking, G., Kim, K., Scuseria, G., Eds.; Elsevier Science: Amsterdam, The Netherlands, 2005.